Vignetting Correction Based on a Two-Dimensional Gaussian Filter With Harmony for Area Array Sensors

Hongtao Cao, Xingfa Gu, Mixia Zhang, Haifeng Zhang, and Xinran Chen

***Abstract*—Vignetting is the main factor causing uneven brightness in an image due to the inherent characteristics of the camera sensor. In radiometric correction-based remote sensing sensors, vignetting can lead to uncomparable radiation signals within and between images, and in the processing of remote sensing images, it leads to an unbalanced color when images are mosaiced. Due to distortions of optical devices, uneven response of detectors and other factors, it is difficult to extract the vignetting from complex reference images and correct it accurately. In this study, a low-pass Gaussion filter was selected to extract the vignetting from reference image, and the standard deviation (STD) and mean of the reference images were used as the factor of harmony to evaluate the strength of the filter for attaining optimal vignetting background. In experiments, the method proposed was compared with polynomial fitting method and general Gaussian filter mothed. The results show that Gaussian filter with harmony method achieves the best effect of vignetting correction compared with the other two methods.**

***Index Terms*—Remote sensing sensors, vignetting, gaussian filter, radiometric calibration.**

I. Introduction

RADIOMETRIC calibration involves establishing a correlation between the digital number (DN) of an optical remote sensor and the illuminance before it is launched into orbit and is the premise for quantitative remote sensing [1], [2]. In the process of radiometric calibration, an inaccurate vignetting correction can lead to radiometric distortion, which causes the brightness of an image to fade from the middle to the edges. Theoretically, vignetting is a phenomenon where the off-axis image points gradually become darker as the light beam reaching the detector plane of the CCD/CMOS becomes gradually narrower due to the existence of an aperture when object points far away from the optical axis are imaged [3]. According to the theory of geometrical optics, it is usually described by the $\cos^4\alpha$ law, which specifies the drop in light intensity depending on the angle formed between a ray of light entering the lens and the optical axis of the lens. Moreover, the defects in the optical components of the sensor can lead to irregular attenuation of the illumination incident on the detector plane of the CCD/CMOS, such as lens distortion, uneven filtering, and optical axis offset [4], [5]. The types of vignetting are listed below in the order corresponding to the light path from a scene to the image sensor: mechanical vignetting, optical vignetting, natural vignetting, and pixel vignetting [6]. For remote sensing analyses, the vignetting effect not only causes uneven brightness and color distortion, but also makes it impossible to compare the radiation features within and between images.

The common vignetting correction methods include the fitting function method and look-up table (LUT) [7]–[9]. The fitting function method uses a polynomial model, an exponential polynomial model, a hyperbolic cosine model, a Gaussian function, or a radial polynomial model to fit the vignetted images obtained under scenes with uniform luminance [10]–[13]; thus, the correction factors for the entire image plane can be calculated. Olsen *et al.* [14] used linear polynomial fitting to correct the optical vignetting of an agriculture camera with two bands developed by the University of North Dakota for deployment on the International Space Station. A nine-order polynomial curve and a six-order polynomial curve with minimal residual variances were selected for the near-infrared and red bands, respectively. Lebourgeois *et al.* [15] established a vignetting correction filter by fitting a polynomial function distribution onto an average image computed over an entire dataset. This vignetting distribution function expresses the vignetting factor for a given position in an image as a polynomial function of the position (i.e., row and column coordinates). The LUT method provides a correction factor for each pixel and has the highest accuracy for vignetting correction. It is a common method to generate the LUT for vignetting correction, where reference images obtained under uniform illumination are used to extract the vignetting background [7], [16]. Subsequently, the vignetting background is used to generate the LUT, which is typically the ratio of the maximum value of the reference image to the value of

Manuscript received 14 December 2021; revised 31 March 2022 and 27 May 2022; accepted 21 June 2022. Date of publication 5 July 2022; date of current version 16 July 2022. This work was supported in part by the National Key R&D Program of China under Grants 2020YFE0200700 and 2019YFE0127300 and in part by the Common Application Support Platform for Land Observation Satellite of National Civil Space Infrastructure under Grant E0A203010F. The associate editor coordinating the review of this manuscript and approving it for publication was Prof. Henry Arguello. (*Corresponding author: Mixia Zhang.*)

Hongtao Cao is with the Aerospace Information Research Institute, Chinese Academy of Sciences, Beijing 100094, China. He is now with the Academy of Ecological Civilization Development for JING-JIN-JI, Tianjin Normal University, Tianjin 300387, China (e-mail: caohongtao0714@163.com).

Xingfa Gu and Xinran Chen are with the Aerospace Information Research Institute, Chinese Academy of Sciences, Beijing 100094, China (e-mail: guxf@radi.ac.cn; chenxr@aircas.ac.cn).

Mixia Zhang is with the Chart Information Center, Tianjin 300450, China (e-mail: zhangmixia0809@163.com).

Haifeng Zhang is with the College of Intelligence and Computing, Tianjin University, Tianjin 300072, China (e-mail: xinyuhuiyin@163.com).

Digital Object Identifier 10.1109/TCI.2022.3188413

each pixel, given the impact of image noise. W. Yu *et al.* [17] used the wavelet denoising method to eliminate the noise in reference images and to improve the accuracy of LUT for anti-vignetting. In implementation of wavelet denoising scheme, the problematic thresholding selection stage had been entirely ignored, and only approximation coefficients are employed in the synthesis stage. F J W-M Leong *et al.* [16] assumed that vignetting is an additive low-frequency signal. Therefore, low-pass filtering can be used to extract it from an image. This filtering can be achieved by convolving the image with a Gaussian kernel. Although this study corrected vignetting to a certain extent, there was an important problem ignored that the strength of filters may disturb the effective of vignetting correction. If the filter is not sufficiently powerful, noise will remain in the vignetting background images. If the filter is too strong, the vignetting background images will be too smooth to eliminate the vignetting effect sufficiently. Due to random noise, quantum response difference, and optical distortion, the vignetting effect is complex [19]–[21], and the strength of the low-pass filter in the LUT method affects the quality of the vignetting correction. Especially, when images are used in radiometric measurement, it is the premise to improve the radiomtric consistency of pixles whether vignetting correction is appropriate.

At present, UAV equipped with near-infrared sensors is used for remote sensing monitoring. The vignetting is obvious and problematic for RS purposes. This study focused on vignetting correction for a near-infrared remote sensor with a complex vignetting effect. To realize an accurate correction, a method based on a Gaussian filter with harmony was used to obtain an accurate LUT for vignetting correction. The strength of the Gaussian filter can be adjusted to adapt to reference images. This method can effectively eliminate noise in images, while maintaining the irregular vignetting features resulting from various factors. In this study, we introduced the main factors and its characteristices of the vignetting effect, and the near-infrared sensor is introduced briefly in Section II.A. Secondly, the strategy of the Gaussian filter adapted to the image proposed was described in Section II.B. The method was to eliminate the vignetting of the near-infrared sensor step by step and the accuracy of the method was evaluated and compared with other methods in Section III. Finally, we discuss and summarize the vignetting correction method in Sections IV and V.

II. Materials and Methods

A. Materials

1) Near-Infrared Sensor: The remote sensing sensor corrected for vignetting is a near-infrared area array sensor with CMOS detectors having a resolution of 1280×960 pixels, and its spectral response range is 400–1000 nm. The digital quantization rate is 16 bit (0-65535). The near-infrared sensor controls the incident light with a narrow-pass filter. The spectral transmittance of the narrow-pass filter is in the range of 820–860 nm. The optical components were fixed focus lenses with a focal length of 8 mm. Fig. 1 shows the structure of the sensor.

Compared to the visible bands, the solar radiation energy in the near-infrared band is weak, and the quantum efficiency of

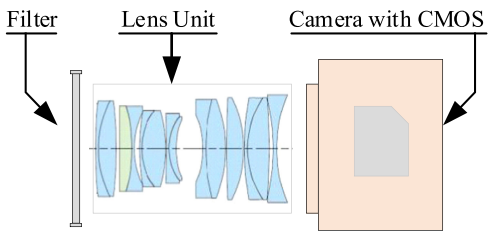

Fig. 1. Structure diagram of a near-infrared sensor.

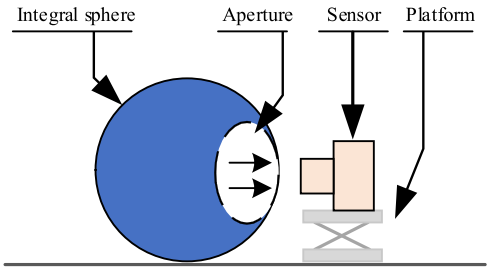

Fig. 2. Integrating sphere and layout of the experimental data acquisition system.

the general the CCD/CMOS sensor is low in the near-infrared band [22]. And particularly, the vignetting of area array sensor is more complex than that of linear array. Therefore, the impact of vignetting in the NIR area array band is more evident.

2) Experimental Instruments: Accurately measuring the vignetting requires a uniform luminance. An integrating sphere was selected to output the uniform field of the luminance [23]. The integrating sphere used in the experiment was XTH2000 produced by Labsphere Inc (New Hampshire, USA). The sphere provided a stable and uniform optical radiation in the wavelength range of 300–2400 nm. Its aperture was 20 cm, and the optical uniformity was more than 98%. Fig. 2 shows the integrating sphere and the layout of the data acquisition process.

3) Vignetting and Its Characteristics: When the integrating sphere output is stable, the sensor looks at the aperture of the integrating sphere and collects the brightness images. Three groups of images with low brightness (quantized value: 0–15000), medium brightness (quantized value: 15000–30000), and high brightness (quantized value: 30000–60000) were collected under different output powers of the integrating sphere. To avoid the slightly uneven brightness of the integrating sphere, each group of images was collected twice in the vertical and horizontal positions of the sensor. In this study, we selected the vignetting of the high-brightness image as the object of introduction; the processing of the low-brightness and medium-brightness vignetted images is similar. Fig. 3 shows the vignetted images.

As shown in Fig. 3(a), the vignetted image taken by the near-infrared sensor is bright in the middle and dark at the four corners. Moreover, the lower corners of the image are brighter than the upper corners. Due to the imperfections induced during the manufacturing process of the optical device, the optical center of the image is inconsistent with the center of the CCD detector shown in Fig. 3(b).

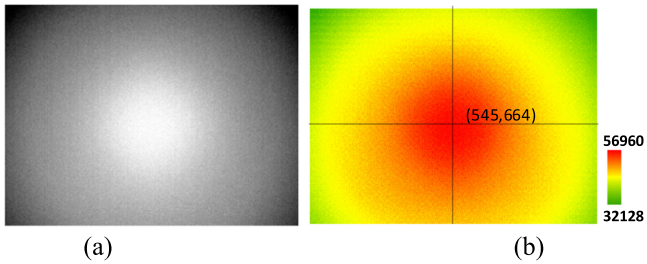

Fig. 3. Vignetted images: (a) Original gray vignetted image; (b) Vignetted image color rendered.

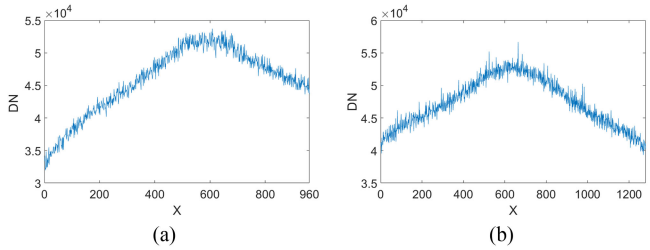

Fig. 4. Characteristics of pixels with the vignetting effect: (a) pixel values of the diagonal of the vignetted image, (b) pixel values of the middle row of the vignetted image.

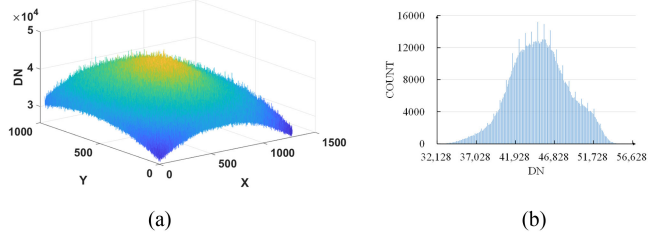

Fig. 5. Random noise in a vignetted image: (a) 3D visualization of vignetting; (b) histogram of image.

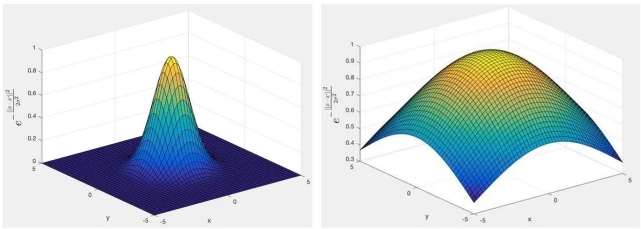

Fig. 6. Two-dimensional Gaussian kernel function when (a) $\sigma = 1$ and (b) $\sigma = 5$.

Fig. 4 shows that vignetting has asymmetric characteristics in terms of the diagonal pixel values, and the vignetting gradient is not smooth. Based on the image statistics, the maximum value of the vignetted image was found to be 3.4 times the minimum value. These vignetting characteristics make it difficult for standard functions to fit it.

We assumed that vignetting of the image is smooth and belongs to the low-frequency component of the image, whereas noise was considered the high-frequency component [15], [16]. Figs. 4 and 5 show that the noise in the vignetted image is random and that it conforms to a normal characteristic. In other words, it belongs to Gaussian noise. This is suitable for Gaussian filtering. Accordingly, it is feasible to eliminate the noise and obtain a smooth vignetting background using the image acquired under uniform luminance of the integrating sphere.

B. Method of Vignetting Correction

1) Low-Pass Gaussian Filter: To eliminate the impact of random noise on the vignetting factors, it is necessary to eliminate the noise before calculating the LUT of the vignetting correction. Here, we choose a low-pass Gaussian filter suitable for Gaussian noise to eliminate the random noise in the vignetted image and obtain a smooth vignetting background [24]. The expression of the Gaussian kernel (radial basis function (RBF)) is as follows [25], [26]:

$$\mathrm{G}\left(\mathrm{x},\mathrm{y}\right) = \frac{1}{2\pi\sigma^2} e^{-\frac{x^2+y^2}{2\sigma^2}} \tag{1}$$

$\mathrm{G}(\mathrm{x},\mathrm{y})$ is the Gaussian kernel function;
x, y is the location of the pixels;
σ is the standard deviation, depends on image features and the smoothness desired.

Based on the RBF, the width of the Gaussian filter, which determines the degree of smoothness, is represented by the parameter σ, and the relationship between σ and the degree of smoothness is simple. The greater the σ value, the wider the band of the Gaussian filter and the better the degree of smoothness [26], [27], as shown in Fig. 6. By adjusting the smoothing degree parameter σ, we can achieve a compromise between the over blurring (over smoothing) of the image features and the many undesirable abrupt variables (under smoothing) caused by noise and fine textures in the smoothed image.

2) Building Filters With Harmony: For vignetted images with different brightness values, we expect that the filter strength can not only effectively eliminate noise, but also help retain the vignetting characteristics and brightness of the original images as much as possible when filtering. Therefore, it is important to control the parameter σ of the Gaussian filter to adapt to vignetted images.

The smoother the image, the lower the image variance. The greater the strength of the Gaussian low filter, the lower the average value of the image. Here, the smoothing degree of the vignetting background is evaluated using the standard deviation (STD) and mean of the images(MEAN). Thus, we expect to establish a functional relationship $f(\sigma)$, $g(\sigma)$ between the filter parameter σ and the STD and MEAN of the vignetting background.

$$STD = f\left(\sigma\right) \tag{2}$$

$$MEAN = g\left(\sigma\right) \tag{3}$$

Based on the above analysis, we predict that the variance of the vignetted image is positively correlated with the Gaussian filter parameter σ. When σ is sufficiently high, the high-frequency information passes through completely, and the variance remains unchanged. The relationship between the mean value of the vignetted image and the Gaussian filter parameter σ is similar. We selected a vignetted image and analyzed the correlation

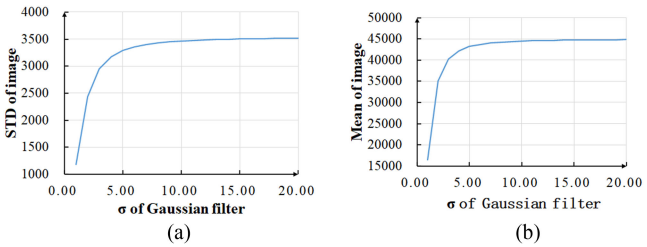

Fig. 7. Relationship between the filter parameter σ and the STD and MEAN of the vignetting background: (a) Trend chart of the variance between the filter parameter σ and vignetting background; (b) Trend chart of the filter parameter σ and mean value of the vignetting background.

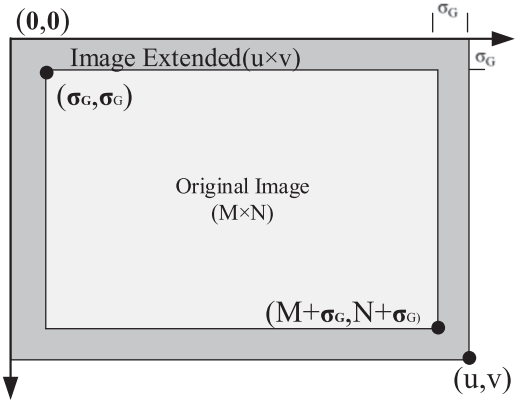

Fig. 8. Image expansion diagram.

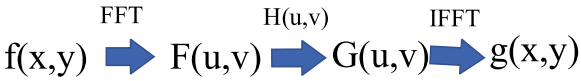

Fig. 9. Flowchart of Gaussian filtering in the frequency domain.

between the parameter σ of the Gaussian filter and the mean and STD of the image. Fig. 7 shows this correlation.

As shown in Fig. 7, the correlation is consistent with the above prediction. Therefore, the change rate of the correlation is used as the judgment factor for the Gaussian filter harmony. Filtering inevitably causes the distortion of image information. Here, D_{std} and D_{mean} is defined as the factors to weigh image distortion.

$$\mathrm{D_{std}} = \frac{\mathrm{STD_{vb}}}{\mathrm{STD_{or}}} \tag{4}$$

$$\mathrm{D_{mean}} = \frac{\mathrm{MEAN_{vb}}}{\mathrm{MEAN_{or}}} \tag{5}$$

$\mathrm{STD_{vb}}$ and $\mathrm{MEAN_{vb}}$ are the STD and MEAN of image filtered by the Gaussian filter respectively; $\mathrm{STD_{or}}$ and $\mathrm{MEAN_{or}}$ are the STD and MEAN of original image respectively.

We expect that the smaller the distortion, the better, when the image noise is fully eliminated by Gaussian filter. As seen in Fig.7, when σ decreases to a certain extent, the decrease of STD and MEAN gradually intensifies. The parameters $\mathrm{D_{std}}$, $\mathrm{D_{mean}}$ of image distortion shall not be less than 99%, following formula is used to control the change.

$$\sigma_{\mathrm{G}} = \mathrm{MIN}\,(\sigma)\ \ \mathrm{D_{std}} > \ 99\% \text{ and } \mathrm{D_{mean}} > 99\% \tag{6}$$

σ_{G} is the min of σ, when $\mathrm{D_{std}} > \ 99\%$ and $\mathrm{D_{mean}} > 99\%$.

3) Extending Image-Edge: The filter may be beyond the image. Therefore, the extension method is often used to solve the outer boundary problem. There are four common methods: zero filling, repetition, symmetry, and circulation. In this research, the repetition method was selected to supplement the border. The rules are as follows:

1) The expansion distance of the four edges of the image is the integer of σ_{G};
2) The row is first expanded and then the column, or vice versa;
3) The repeated value is the boundary pixel value of the original image, and the equation is as follows:

$$\mathrm{I_{ext}}\,(\mathrm{u},\mathrm{v}) = \begin{cases} \mathrm{I_{original}}\,(\mathrm{u},\mathrm{v}) & \mathrm{u} \le [\sigma_{\mathrm{G}}]\,, \mathrm{v} \le [\sigma_{\mathrm{G}}] \\ \mathrm{I_{original}}\,(\mathrm{u}-[\sigma_{\mathrm{G}}]\,, \mathrm{v}-[\sigma_{\mathrm{G}}]) & [\sigma_{\mathrm{G}}] < \mathrm{u} \le \mathrm{M}+[\sigma_{\mathrm{G}}]\,, \\ & [\sigma_{\mathrm{G}}] < \mathrm{v} \le \mathrm{N}+[\sigma_{\mathrm{G}}] \\ \mathrm{I_{original}}\,(\mathrm{u}-2\sigma_{\mathrm{G}}, \mathrm{v}-2\sigma_{\mathrm{G}}) & \mathrm{u} > \mathrm{M}+[\sigma_{\mathrm{G}}] \\ xs, & \mathrm{v} > \mathrm{N}+[\sigma_{\mathrm{G}}] \end{cases} \tag{7}$$

$\mathrm{I_{original}}$ is the original image which has not been extended;
$\mathrm{I_{ext}}$ is the image extended;
u, v is the location of pixel. Fig. 8 is used to display the mode of image expansion.

4) Filtering in the Frequency Domain: Gaussian filtering of a vignetted image is performed in the frequency domain to improve the efficiency. First, the image is transformed by Fourier transform (FFT) and filtered using the Gaussian filter (GF). The inverse Fourier transform (IFFT) is used to transform the image [25], [28]. The process of Gaussian filtering in the frequency domain is shown in Fig. 9.

f(x,y) is the original images in spatial domain; F(u,v) is the images in frequency domain; G(u,v) is the images filtered by Gaussion function in frequency domain; g(x,y) is the images which has been filtered and converted back to spatial domain.

5) Normalization and Equalization: The vignetted image is normalized as the correction factors [15], [29].

$$Norm\_V\ \ (x,y) = \frac{I\,(x,y)}{I_{max}} \tag{8}$$

$I(x,y)$ is the pixel value in the vignetting background; I_{max} is the maximum pixel value within the vignetted image; $Norm\_V(x,y)$ is the factor of vignetting correction normalized; x, y is the location of pixel.

Several normalized vignetted images were obtained at different incident radiation levels. The effective LUT of vignetting correction is the mean image of these images.

The method and experiments described in the paper are implemented according to the flow of Fig. 10.

III. Results

A. Harmony of Gaussian Filter

Based on the method described in Section II.B, the correlation between the STD and the mean value of the three vignetted

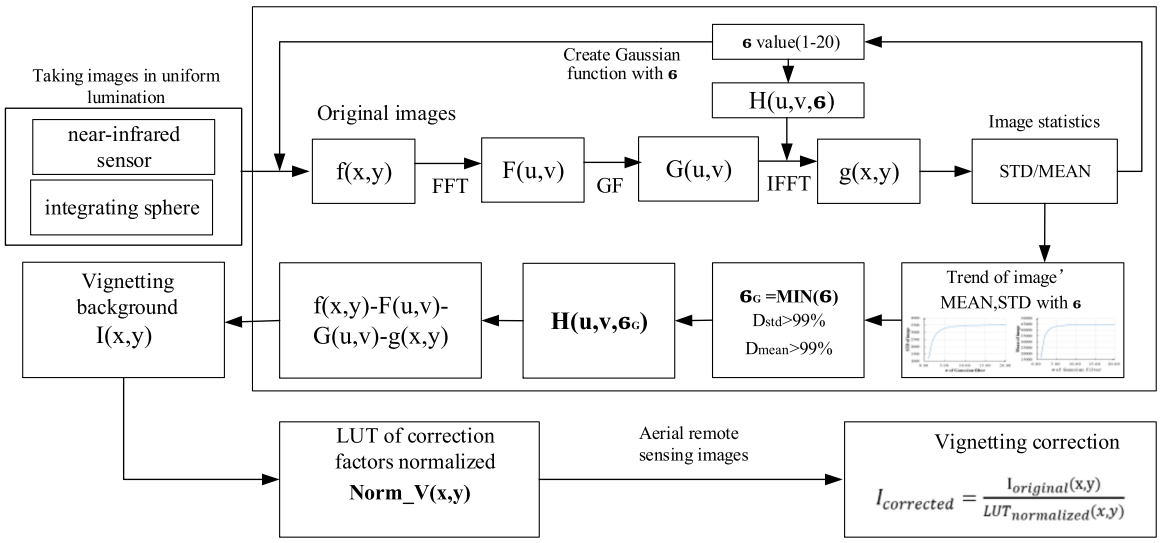

Fig. 10. Flow chart of implementation.

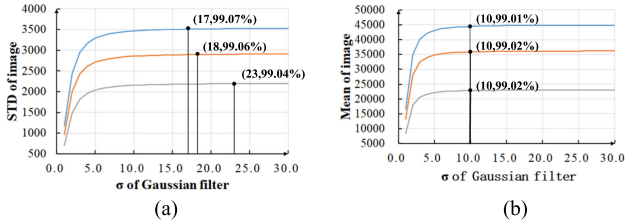

Fig. 11. Correlation between the STD and mean value of the vignetted image and Gaussian filter parameter σ: (a) Correlation between the STD of the vignetted image and Gaussian filter parameter σ and the value of σ satisfying the requirement; (b) Correlation between the mean of the vignetted image and Gaussian filter parameter σ and the value of σ satisfying the requirement.

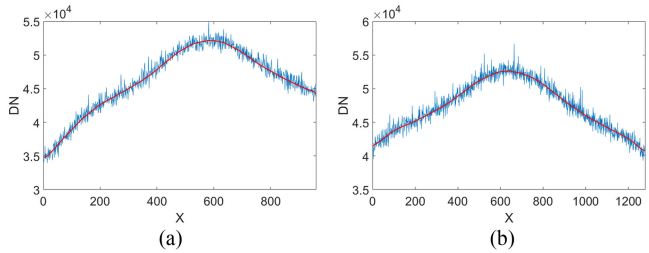

Fig. 12. Fitting performance of vignetting background with high brightness when $\sigma = 17$ (red) and original vignetted image (blue): (a) Pixel value of the diagonal of the image; (b) Pixel values of the middle row of the image.

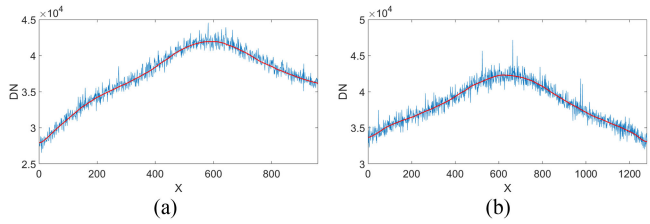

Fig. 13. Fitting performance of vignetting background with medium brightness when $\sigma = 18$ (red) and original vignetted image (blue): (a) Pixel values of the diagonal of the image; (b) Pixel values of the middle row of the image.

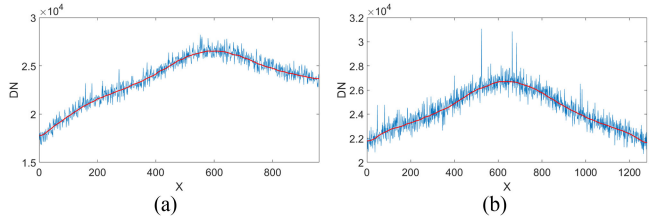

Fig. 14. Fitting performance of vignetting background with low brightness when $\sigma = 23$ (red) and original vignetted image (blue): (a) Pixel value of the diagonal of the image; (b) Pixel values of the middle row of the image.

images with different brightness values and the Gaussian filter parameter σ is calculated and shown in Fig. 11. The value of the parameter σ was determined based on the conditions of $D_{std} > 99\%$ and $D_{mean} > 99\%$.

After filtering using the Gaussian filter with harmony in the frequency domain, a smooth vignetting background was obtained. Figs. 12, 13, and 14 show the fitting performance of the vignetting background and original vignetted images.

As shown in the figures above, the noise in the vignetted image with different brightness values was eliminated, and the vignetting features were preserved. The vignetting background effectively fits the vignetted image.

Moreover, another near-infrared camera was selected for further experiments to confirm the practicability of the method. The near-infrared camera had 964×1292 pixels, and its band response range was 740–760 nm with quantization of 12 bits. Fig. 15 shows the adaptive parameter σ of the Gaussian filter.

After the harmony analysis, the Gaussian filter with the parameter $\sigma = 14$ was used for vignetting correction. Fig.16 shows

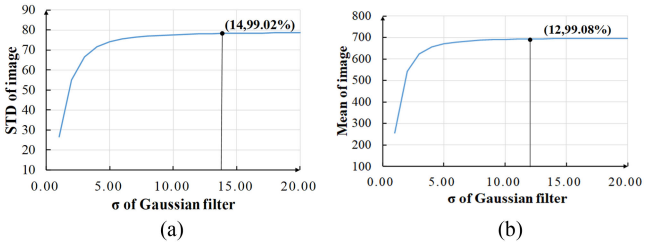

Fig. 15. Adaptive parameter σ of the Gaussian filter for 740–760 nm near-infrared camera: (a) Correlation between the STD of vignetted image and Gaussian filter parameter σ and the value of σ satisfying the requirement; (b) Correlation between the MEAN of the vignetted image and Gaussian filter parameter σ and the value of σ satisfying the requirement.

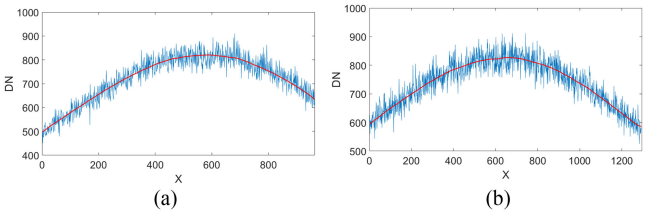

Fig. 16. Fitting performance of vignetting background with low brightness when $\sigma = 14$ (red) and original vignetted image (blue): (a) Pixel values of the diagonal of the image; (b) Pixel values of the middle row of the image.

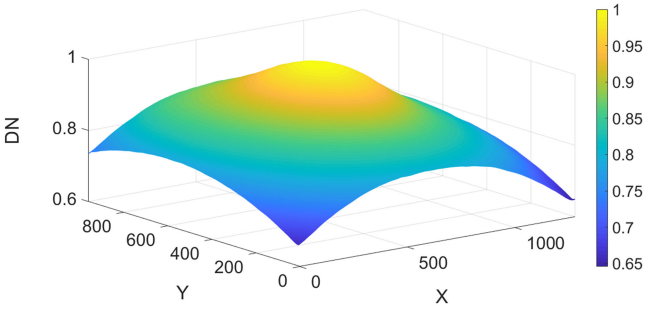

Fig. 17. Normalized LUT of vignetting correction factors.

the fitting performance of the vignetting background and original vignetted image.

Fig. 16 shows that the Gaussian filter with the proposed harmony achieves a good fitting effect.

B. LUT Obtained By Gaussian Filter With Harmony

Multiple vignetting backgrounds with different brightness values were normalized and averaged. Fig. 17 shows the final normalized vignetting correction factor.

The LUT normalized recorded the correction factors of the vignetting correction for each pixel. When correcting an image, the pixel value of the image $\mathrm{I}_{original}$ is used to divide the correction factors $\mathrm{I}_{original}$ of the corresponding position (x, y) in the LUT [30], [31].

$$I_{corrected} = \frac{\mathrm{I}_{original}\,(\mathrm{x}, \mathrm{y})}{LUT_{normalized}\,(x, y)} \tag{9}$$

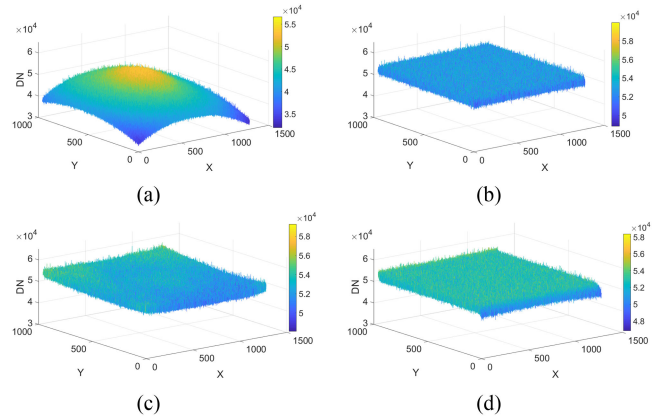

Fig. 18. Comparing the performance of vignetting correction methods: (a) Original image; (b) Image corrected by Gaussian filter with harmony when $\sigma = 14$; (c) Image corrected by polynomial fitting method; (d) Image corrected by general Gaussian filter when $\sigma = 8$.

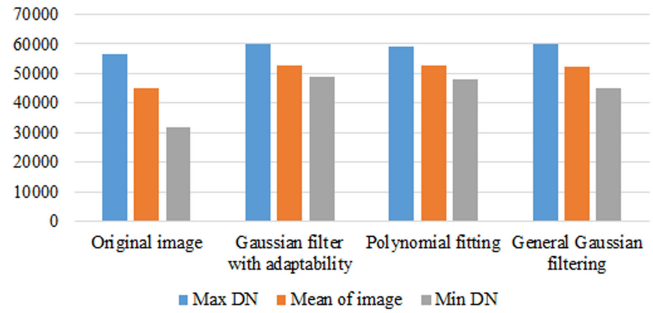

Fig. 19. Maximum, average and minimum values of corrected image and original image.

C. Comparison With Conventional Method

To validate the performance of the method proposed, we compared it with the conventional methods. The polynomial fitting method and general Gaussian filtering method were used for vignetting correction. The polynomial fitting equation [9], [14], [32] is as follows:

$$f\ (x) = p1 * r(x,y)^6 + p2 * r(x,y)^5 + p3 * r(x,y)^4 + p4 * r(x,y)^3 + p5 * r\,(x,y)^2 + p6 * r\,(x,y) + p7 \tag{10}$$

$$r\,(x,y) = \sqrt{(\mathrm{x} - \mathrm{centerX})^2 + (\mathrm{y} - \mathrm{centerY})^2} \tag{11}$$

Here, $r(x, y)$ is the distance from the pixel (x, y) to the optical center ab $(centerX, centerY)$, and $p1 - p7$ represent the coefficients of the polynomial fitting.

Fig. 18 shows that the three methods are effective for vignetting correction. Comparing the performance of vignetting correction in Fig. 18(b), (c), and (d), we find that the image corrected by the Gaussian filter with harmony is the smoothest. Figs. 19 and 20 presents the statistical characteristics of the original and corrected images.

As shown in Fig. 19, the deviation of maximum, average and minimum values of image corrected by the method proposed is

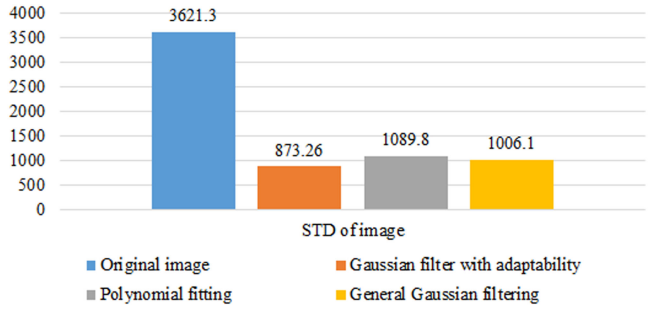

Fig. 20. STDs of corrected image and original image.

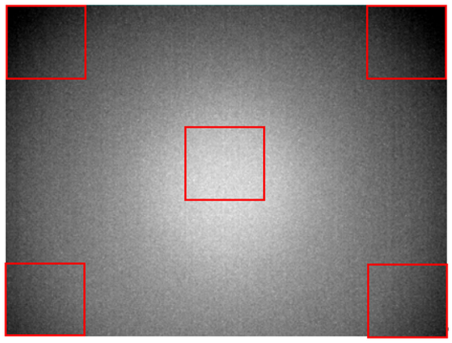

Fig. 21. Five districts in images.

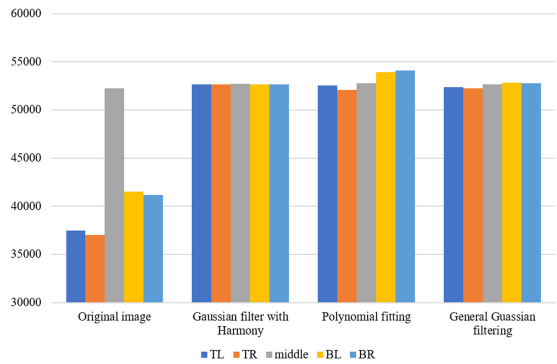

Fig. 22. Maximum, average and minimum values of corrected image and original image.

the smallest. In Fig. 20, the standard deviation (STD) of the image corrected by the Gaussian filter with harmony is the lowest. These demonstrates that the DN of pixels in image corrected by the proposed method are the most balanced. Overall, the Gaussian filter with harmony proposed for vignetting correction exhibited the best performance.

Furthermore, five districts(100×100 pixel window) of image were extracted to comparing the mean value and STD of them. The five districts are top left(TL), top right(TR), middle, bottom left(BL), bottom right(BR) respectively, as shown in Fig. 21.

Fig. 22 shows that the mean values of five districts in image corrected using Gaussian filter with harmony were almost equal; Fig. 23 shows that the STDs of five districts in image corrected using Gaussian filter with harmony were the lest. Therefore, we can be fully convinced that Gaussian filter with harmony has

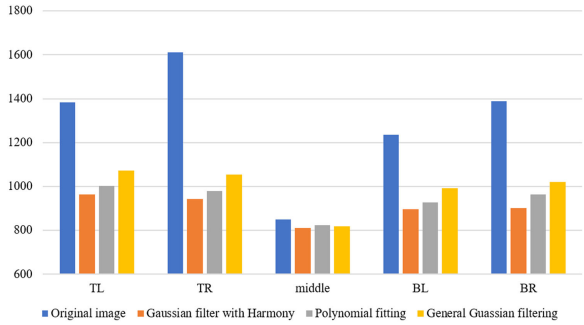

Fig. 23. STDs of five districts in original image image corrected with three methods.

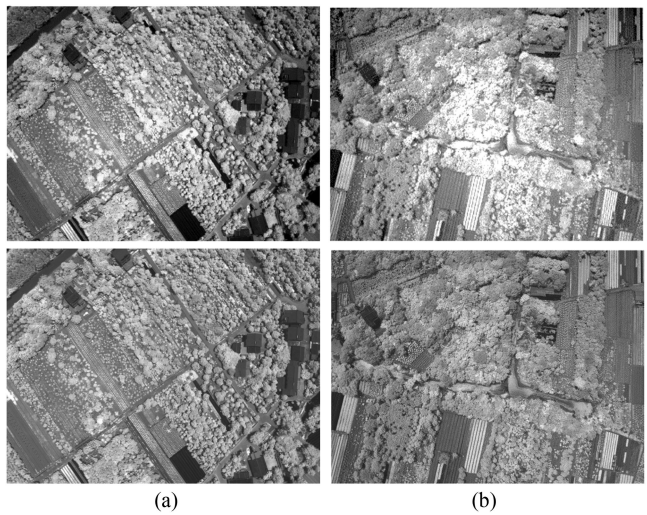

Fig. 24. Aerial remote sensing images obtained by the near-infrared sensor: (a) Original image; (b) Corrected image.

achieved good vignetting correction effect both globally and locally.

D. Validating the Performance of LUT

Aerial remote sensing images obtained using the near-infrared sensor based on an unmanned aerial vehicle were used to test the actual performance. Fig. 24 shows the images before and after the correction.

The brightness of the aerial remote sensing image becomes more balanced after correction. In particular, the contrast at the four corners and in the middle of the image was reduced. This confirms the effectiveness of the proposed vignetting correction method.

IV. Discussion

Vignetting correction is the most important task in the radiometric calibration and image dodging of the remote sensing sensor. In addition to causing visual imbalance, the correction accuracy directly determines the performance of remote sensing quantitative inversion and image interpretation. Moreover, with the wide application of computer vision technology in target detection and defect recognition, vignetting also brings challenges to the rationality of the recognition algorithm and algorithm

parameters. Effectively eliminating the vignetting effect will promote the development and application of the remote sensing technology and computer vision technology.

Currently, the function fitting method is commonly used for the vignetting correction of sensors, while this type of ideal equation cannot completely eliminate irregular vignetting. In particular, it is difficult to fit near-infrared and thermal infrared images exhibiting a more complex vignetting effect. The LUT method has the best vignetting correction accuracy, because it provides each pixel with the most appropriate correction factor. To avoid the impact of image random noise and response noise, the image filtering algorithm is often used in vignetted image processing to obtain a smooth vignetting background when calculating the LUT of the vignetting correction. The key to obtain an accurate LUT is to adjust the filter strength reasonably, which is ignored in most of the current vignetting correction research. Therefore, we proposed a Gaussian filter with harmony for vignetting correction. The method proposed was to determine the optimal parameter σ of the Gaussian filter kernel using the relationship between it and the STD and mean of the images. Through experiments, we found that the vignetting background obtained using this method fits the original vignetting image well and achieves a good vignetting correction. Furthermore, this method is suitable for filtering vignetted images with different brightness values of the same sensor, as well as vignette images of other sensors, such as visible light remote sensing sensors and digital cameras.

In addition, this method requires a lot of calculation to find the optimal fitness value. We will improve the computational efficiency in further research. And the step of the σ may caused deviation, need to be researched future.

V. Conclusion

The Gaussian filter with harmony is a simple and efficient method for vignetting correction and can be used to obtain a high-precision LUT for vignetting correction. The harmony helps avoid the cumbersome task of repeated parameter adjustment experiments and the deviation due to unreasonable parameters. This method can quickly determine the optimal Gaussian filter parameter for different images and different sensors. Compared with the polynomial fitting method and the general Gaussian filtering, the images corrected using the Gaussian filter with harmony were found to be smoother, and the standard deviation was lower. The mean values of five districts in image corrected using Gaussian filter with harmony were almost equal; And the STD of five districts in image corrected using Gaussian filter with harmony were the lest.

V. Disclosures

The authors declare no conflicts of interest.

References

[1] V. Lebourgeois, A. Bégué, S. Labbé, B. Mallavan, L. Prévot, and B. Roux, "Can commercial digital cameras be used as multispectral sensors? A crop monitoring test," *Sensors-Basel*, vol. 8, no. 11, pp. 7300–7322, 2008, doi: 10.3390/s8117300.

[2] E. Nocerino, M. Dubbini, F. Menna, F. Remondino, M. Gattelli, and D. Covi, "Geometric calibration and radiometric correction of the MAIA multispectral camera," *Int. Arch. Photogrammetry, Remote Sens. Spatial Inf. Sci.*, vol. XLII-3/W3, pp. 149–156, 2017, doi: 10.5194/isprs-archives-XLII-3-W3-149-2017.

[3] P. B. Catrysse, X. Liu, and A. El Gamal, "QE reduction due to pixel vignetting in CMOS image sensors," *Sensors Camera Syst. Scientific, Ind., Digit. Photography Appl.*, vol. 3965, pp. 420–430, 2000, doi: 10.1117/12.385460.

[4] Y. Zheng, C. Kambhamettu, and S. Lin, "Single-image optical center estimation from vignetting and tangential gradient symmetry," in *Proc. IEEE Conf. Comput. Vis. Pattern Recognit.*, 2009, pp. 2058–2065. [Online]. Available: https://go.exlibris.link/1LkkC2lV, doi: 10.1109/CVPR.2009.520674.

[5] J. Shin and T. Sakurai, "Vignetting effect in the soft X-ray telescope onboard Yohkoh: I. Numerical simulation," *Sol. Phys.*, vol. 290, no. 5, pp. 1531–1546, 2015, doi: 10.1007/s11207-013-0292-x.

[6] M. Brady and G. E. Legge, "Camera calibration for natural image studies and vision research," *J. Opt. Soc. Amer. Opt. Image Sci. Vis.*, vol. 26, no. 1, pp. 30–42, 2009, doi: 10.1364/josaa.26.000030.

[7] D. Lee, C. Yang, Y. Park, and C. Kim, "A camera-based color calibration of tiled display systems under various illumination environments," *J. Inf. Display*, vol. 18, no. 2, pp. 73–85, 2017, doi: 10.1080/15980316.2017.1291454.

[8] L. Zhaolong, S. Tongsheng, and L. Shuli, "Vignetting correction method for the infrared system based on polynomial approximation," *Infrared Laser Eng.*, vol. 45, no. B05, 2016, Art. no. 5.

[9] A. Kordecki, A. Bal, and H. Palus, "A smooth local polynomial model of vignetting," in *Proc. Int. Conf. Methods Models Automat. Robot.*, 2017, pp. 878–882.

[10] A. Kordecki, H. Palus, and A. Bal, "Practical vignetting correction method for digital camera with measurement of surface luminance distribution," *Signal, Image Video Process.*, vol. 10, no. 8, pp. 1417–1424, 2016, doi: 10.1007/s11760-016-0941-2.

[11] W. Yu, "Practical anti-vignetting methods for digital cameras," *IEEE Trans. Consum. Electron.*, vol. 50, no. 4, pp. 975–983, Nov. 2004, doi: 10.1109/TCE.2004.1362487.

[12] I. A. Konyakhin, A. M. Sakhariyanova, R. Li, F. Wyrowski, J. T. Sheridan, and Y. Meuret, "Design the algorithm compensation of vignetting error at optical-electronic autoreflection system by modelling vignetted image," *Proc. Int. Soc. Opt. Photon.*, vol. 9889, 2016, Art. no. 988915-988915-7, doi: 10.1117/12.2225883.

[13] V. F. Duma, "Radiometric versus geometric, linear, and nonlinear vignetting coefficient," *Appl. Opt.*, vol. 48, no. 32, pp. 6355–6364, 2009, doi: 10.1364/AO.48.006355.

[14] D. Olsen, C. Dou, X. Zhang, L. Hu, H. Kim, and E. Hildum, "Radiometric calibration for AgCam," *Remote Sens.-Basel*, vol. 2, no. 2, pp. 464–477, 2010, doi: 10.3390/rs2020464.

[15] V. Lebourgeois, A. Bégué, S. Labbé, B. Mallavan, L. Prévot, and B. Roux, "Can commercial digital cameras be used as multispectral sensors? A crop monitoring test," *Sensors-Basel*, vol. 8, no. 11, pp. 7300–7322, 2008, doi: 10.3390/s8117300.

[16] H. Cao, X. Gu, X. Wei, T. Yu, and H. Zhang, "Lookup table approach for radiometric calibration of miniaturized multispectral camera mounted on an unmanned aerial vehicle," *Remote Sens. (Basel, Switzerland)*, vol. 12, no. 4012, 2020, Art. no. 4012, doi: 10.3390/rs12244012.

[17] W. Yu, Y. Chung, and J. Soh, "Vignetting distortion correction method for high quality digital imaging," in *Proc. 17th Int. Conf. Pattern Recognit.*, 2004, vol. 3, pp. 666–669. [Online]. Available: https://go.exlibris.link/f2cRRkf2, doi: 10.1109/ICPR.2004.133461.

[18] F. J. W. Leong, M. Brady, and J. O. D. McGee, "Correction of uneven illumination (vignetting) in digital microscopy images," *J. Clin. Pathol.*, vol. 56, no. 8, pp. 619–621, 2003, doi: 10.1136/jcp.56.8.619.

[19] S. Lyu, "Estimating vignetting function from a single image for image authentication," in *Proc. 12th ACM Workshop Multimedia Secur.*, 2010, pp. 3–12. [Online]. Available: https://go.exlibris.link/5QQ0Ft4q, doi: 10.1145/1854229.185423.

[20] M. Aggarwal, H. Hua, and N. Ahuja, "On cosine-fourth and vignetting effects in real lenses," in *Proc. 8th IEEE Int. Conf. Comput. Vis.*, 2001, vol. 1, pp. 472–479. [Online]. Available: https://go.exlibris.link/2W9Cpw1H, doi: 10.1109/ICCV.2001.937554.

[21] Z. Wang and X. Xiong, "Characterization of MODIS SD screen vignetting function using observations from spacecraft yaw maneuvers," *Proc. Int. Soc. Opt. Photon.*, vol. 7452, pp. 745217–7452112, 2009, [Online]. Available: https://go.exlibris.link/bmtHMNR3, doi: 10.1117/12.82465.

[22] H. Cao, X. Gu, Y. Sun, H. Gao, Z. Tao, and S. Shi, "Comparing, validating and improving the performance of reflectance obtention method for UAV-Remote sensing," *Int. J. Appl. Earth Observ. Geoinf.*, vol. 102, 2021, Art. no. 102391, doi: 10.1016/j.jag.2021.102391.
[23] Y. Lu, K. Wang, and G. Fan, "Photometric calibration and image stitching for a large field of view multi-camera system," *Sensors-Basel*, vol. 16, no. 4, 2016, Art. no. 516, doi: 10.3390/s16040516.
[24] G. Deng and L. W. Cahill, "An adaptive Gaussian filter for noise reduction and edge detection," in *Proc. IEEE Conf. Rec. Nucl. Sci. Symp. Med. Imag. Conf.*, 1993, vol. 3, pp. 1615–1619. [Online]. Available: https://go.exlibris.link/znbKFDQQ, doi: 10.1109/NSSMIC.1993.37356.
[25] J. Wang, G. Wu, J. Li, and S. K. Jha, "A new method estimating linear Gaussian filter kernel by image PRNU noise," *J. Inf. Secur. Appl.*, vol. 44, pp. 1–11, 2019, doi: 10.1016/j.jisa.2018.11.002.
[26] M. Wang, S. Zheng, X. Li, and X. Qin, "A new image denoising method based on Gaussian filter," in *Proc. Int. Conf. Inf. Sci. Electron. Elect. Eng.*, 2014, vol. 1, pp. 163–167.
[27] G. Gómez, "Local smoothness in terms of variance: The adaptive Gaussian filter," in *Proc. Brit. Mach. Vis. Conf.*, Sep. 2000, pp. 1–10.
[28] H. kai, T. Pingfan, and W. Chengyou, " Image vignetting restoration method based on Gaussian surface fitting," *J. Electron.*, vol. 37, no. 1, pp. 67–71, 2009, doi: 10.3321/j.issn:0372-2112.2009.01.012.
[29] K. Bedrich, M. Bokalic, M. Bliss, M. Topic, T. R. Betts, and R. Gottschalg, "Electroluminescence imaging of PV devices: Advanced vignetting calibration," *IEEE J. Photovolt.*, vol. 8, no. 5, pp. 1297–1304, Sep. 2018, doi: 10.1109/JPHOTOV.2018.2848722.
[30] R. Minařík and J. Langhammer, "Rapid radiometric calibration of multiple camera array using in-situ data for uav multispectral photogrammetry," *Int. Arch. Photogrammetry, Remote Sens. Spatial Inf. Sci.*, vol. XLII-2/W17, pp. 209–215, 2019, doi: 10.5194/isprs-archives-XLII-2-W17-209-2019.
[31] A. Kordecki *et al.*, "A study of vignetting correction methods in camera colorimetric calibration," *Proc. Int. Soc. Opt. Photon.*, vol. 10341, 2017, Art. no. 103410X-103410X-5. [Online]. Available: https://go.exlibris.link/vx2zDK7d, doi: 10.1117/12.226853.
[32] Y. Zheng, J. Yu, S. B. Kang, S. Lin, and C. Kambhamettu, "Single-image vignetting correction using radial gradient symmetry," in *Proc. IEEE Conf. Comput. Vis. Pattern Recognit.*, 2008, pp. 1–8. [Online]. Available: https://go.exlibris.link/2Ml2ns8S, doi: 10.1109/CVPR.2008.4587413.

Hongtao Cao received the Ph.D. degree from Aerospace Information Research Institute, Chinese Academy of Sciences, Beijing, China, in June 2022. He is currently a Research Assistant with the Academy of Ecological Civilization Development for JING-JIN-JI, Tianjin Normal University, Tianjin, China. His research interests include computational imaging, remote sensing radiometric calibration, and image processing.

Xingfa Gu photograph and biography not available at the time of publication.

Mixia Zhang photograph and biography not available at the time of publication.

Haifeng Zhang photograph and biography not available at the time of publication.

Xinran Chen photograph and biography not available at the time of publication.